PERGAMON

International Journal of Multiphase Flow 28 (2002) 757–772

International Journal of Multiphase Flow

www.elsevier.com/locate/ijmulflow

Air–water two-phase flow and heat transfer in a plate heat exchanger

P. Vlasogiannis, G. Karagiannis, P. Argyropoulos, V. Bontozoglou *

Department of Mechanical and Industrial Engineering, University of Thessaly, Pedion Areos, GR-38334 Volos, Greece

Received 21 February 2001; received in revised form 31 December 2001

Abstract

A plate heat exchanger is tested under two-phase flow conditions by using an air/water mixture as the cold stream. Visual observations recorded by a high-speed video camera lead to the construction of a flow regime map. The heat transfer coefficient of the air/water stream is measured as a function of air and water superficial velocities. The flow regime with a gas-continuous phase covering the core of the channel and liquid flowing in the form of rivulets inside the furrows shows particularly favorable heat transfer characteristics. © 2002 Elsevier Science Ltd. All rights reserved.

Keywords: Air-water flow; Plate and Frame heat exchanger; Flow regime map; Coefficient of heat transfer

1. Introduction

Plate and frame heat exchangers are frequently employed in the food and chemical process industry, replacing tubular heat exchangers in several traditional duties. They are attractive because of operational flexibility, high heat transfer efficiency per unit volume and ease of inspection and cleaning (Usher, 1970; Marriott, 1971; Walker, 1982; Carlson, 1992).

Plate heat exchangers are primarily used in liquid-to-liquid heat exchange duties. Thus, performance in single-phase applications has been documented in the open literature (Buonopane et al., 1963; Cooper and Usher, 1983; Raju and Bansal, 1983; Focke et al., 1985; Shah and Focke, 1988; Bansal and Müller-Steinhagen, 1993) to an extent that enables reliable design and rating calculations.

More recently, the use of plate heat exchangers in evaporation and condensation duties has been advocated (Patel and Thompson, 1991). The application is motivated by the closer temperature

* Corresponding author. Tel.: +30-421-74069; fax: +30-421-74050.
E-mail address: bont@mie.uth.gr (V. Bontozoglou).

0301-9322/02/$ - see front matter
PII: S0301-9322(02)00010-1

approach and the more uniform residence time, which characterize the operation of plate exchangers in comparison to shell-and-tube exchangers. Consolidated progress in this direction requires an understanding of gas/liquid two-phase flow in the flow passages of the plate heat exchanger (which deviate remarkably from the much-studied tubular geometry) and of the effect of the adopted flow regimes on the heat transfer characteristics.

To the best of our knowledge, the above problem has not yet been sufficiently addressed in the open literature. A recent related work is the study by Gradeck and Lebouché (2000) of the gas–liquid flow patterns in horizontal corrugated channels. It is also interesting to note that satisfactory understanding of even the fundamental problem of gas/liquid film flow over a corrugated surface, and of the effect of the corrugation parameters (wavelength, amplitude, shape) is presently lacking. The few studies that have addressed aspects of the fundamental problem (Focke and Knibbe, 1986; Shetty and Cerro, 1993; Bontozoglou and Papapolymerou, 1997, 1998; Trifonov, 1998; Malamataris and Bontozoglou, 1999) reveal a host of non-trivial phenomena, indicating that further research may prove fruitful.

The present work considers the co-current downward flow of air/water mixtures in the vertical channels of an actual plate heat exchanger. Visual observations of flow regimes are reported, as well as measurements of heat transfer rates to the air/water mixture, which serves as the cold stream in the heat exchanger. The ultimate goal is to delineate the influence of flow regime on heat transfer coefficient. The experimental setup is described in Section 2 and the methodology of data analysis is outlined in Section 3. Section 4 presents visual observations of the flow regimes and Section 5 contains the heat transfer measurements. Finally, some concluding remarks are presented in Section 6.

2. Experimental setup

The experimental setup is shown in Fig. 1. Demineralized water is used as the single-phase, heating medium. It is stored in a 500-l tank and its temperature is regulated by electric resistances driven by a PID controller. Demineralized, cold water constitutes the liquid phase of the gas/liquid mixture and is provided by pumping from a 500-l storage tank. Air is withdrawn from the compressed-air facility of the laboratory and is mixed with the water in a T-joint, located on the pipe leading to the heat exchanger (i.d. = 36 mm), 50 diameters upstream from the entrance port. Typical temperatures of the experiment are: 40 °C for the inlet of the hot water stream and 25 °C for the inlet of the cold air/water stream.

Air and water flow rates are measured by a series of variable-area rotameters. The accuracy is $\pm 2\%$ for the single-phase stream and $\pm 6\%$ for the components of the two-phase stream under the most adverse conditions corresponding to fluctuations due to slug flow inside the exchanger. The pressure at the exit of the air rotameters is recorded and the flow rate is corrected for deviations from standard conditions. Temperatures of the streams entering and exiting the plate heat exchanger are measured by K-type thermocouples (accuracy ± 0.1 °C)—calibrated in the respective temperature range—and are recorded in a data logger.

The plate heat exchanger used in the present study is the Alfa-Laval P-01. It consists of 13 stainless steel plates, assembled for single-pass counter-current flow and providing six flow channels per stream. A layer of glass wool thermally insulates the entire heat exchanger, as well as

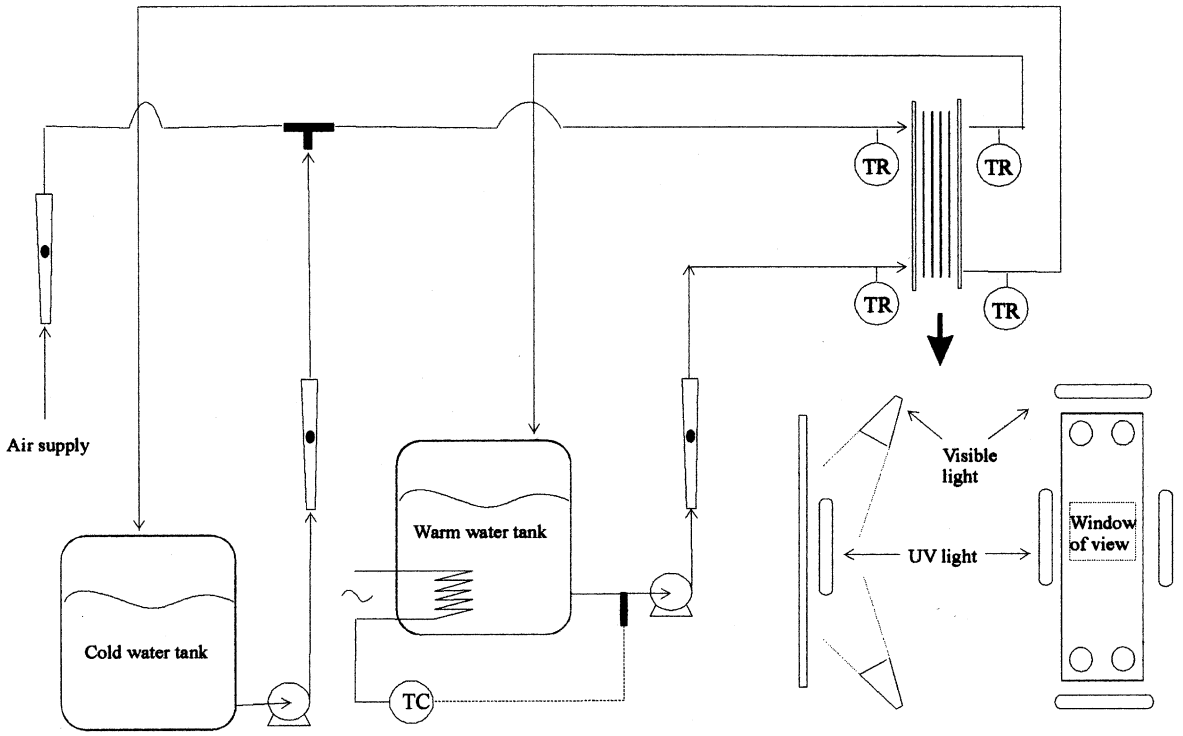

Fig. 1. Outline of the experimental setup, with a front and side view of the position of lighting.

the inlet and outlet ports. The plates, one of which is shown in Fig. 2, have chevron-type corrugations with height 2.4 mm and wavelength (in the direction normal to the crests) 10 mm. The corrugations form a herringbone pattern at an angle of 60° relative to the direction of flow, and

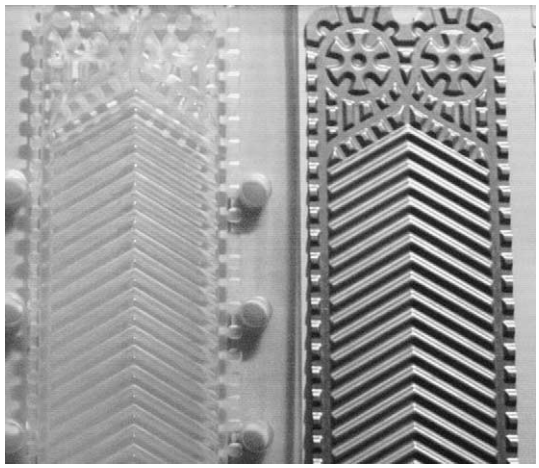

Fig. 2. A steel plate of the P-01 heat exchanger and the plexiglass cover with the embossed corrugation pattern.

Table 1
Plate dimensions

Plate length	0.430 m
Plate width	0.123 m
Mean spacing between plates, b_c	0.0024 m
Plate sheet thickness	0.0006 m
Port-to-port length	0.352 m
Plate width inside gasket, w	0.100 m
Heat transfer area per plate	0.032 m^2
Mean flow cross-section per channel	2.4×10^{-4} m^2

successive plates are arranged with the corrugation pattern pointing in opposite directions. The major dimensions of the plates are summarized in Table 1.

Visual observation of air/water flow is made possible by replacing the movable end cover of the exchanger with a 30 mm-thick plexiglass plate. Using lithographic techniques, the corrugation pattern of a steel plate has been embossed on the inner surface of the plexiglass. Thus, the channel formed between the last plate and the plexiglass cover is visually accessible and has the same geometry as any inner channel. A picture of the plate with the embossed surface pattern is shown in Fig. 2

A RedLake® Motion Scope PCI high-speed video camera is used for recording the images. The camera is connected to a PC-based frame grabber capable of storing 2 s of action, with a speed of up to 1000 frames/s. A fluorescent dye (100 ppm of uranine) is added to the water stream of the two-phase mixture and is irradiated by UV-light to enhance visual contrast between the gas and the liquid phase, thus facilitating observation. The dimensions of the window of view are 75×85 mm^2 and the position of the visible and UV lighting is indicated in Fig. 1.

3. Data analysis

All two-phase flow data are reported in terms of superficial air and water velocities, which are defined from the respective volumetric flow rates, V_G and V_L, and the average flow cross-section, A_f. In particular, the airflow rate is converted to standard temperature and pressure (1 atm and 25 °C). Thus,

$$u_{SG} = \frac{V_G}{A_f} \quad \text{and} \quad u_{SL} = \frac{V_L}{A_f} \tag{1}$$

The average cross-section available for flow is defined, in terms of the plate width inside the gasket, w, the mean spacing between plates, b_c, [1] and the number of channels dedicated to each stream, N, as

[1] The mean spacing between plates is provided by the manufacturer. Alternatively, Eq. (2) may be considered as its definition in terms of channel cross-section and width. The essential property of chevron plates is that they provide a flow passage which, though of variable shape among different cross-sections, has almost constant overall cross-sectional area (Shah and Wanniarachchi, 1991).

$$A_f = wb_c N \tag{2}$$

The Reynolds number is defined, based on the hydraulic diameter

$$D_h = \frac{2wb_c}{w + b_c} \approx 2b_c \tag{3}$$

as follows:

$$Re_i = \frac{\rho_i u_{Si} D_h}{\mu_i} = \frac{2\rho_i V_i}{wN\mu_i}, \quad i = \text{G } or \text{ L} \tag{4}$$

The range of superficial velocities of the two-phase mixture covered by the present experiments is $u_{SL} = 0.01$–0.25 m/s and $u_{SG} = 0.3$–10 m/s.

Flow regimes are defined visually. More specifically, the optical setup permits us to differentiate between a liquid-continuous phase and a gas-continuous phase by the difference in reflection intensity from the surface of the stainless steel plate. In particular, regions of the visually accessible channel occupied by gas appear as bright and reflective, whereas regions occupied by liquid are blurry. Representative examples (to be discussed in Section 4) are provided by Fig. 4 for the former and Fig. 5 for the latter. The flow regimes to be subsequently described are observed under isothermal conditions and using a single isolated downward flow passage, in order to avoid the effects of possible maldistribution among multiple passages.

The heat load in the non-isothermal experiments is calculated by applying an energy balance for the hot stream, which always consists of pure water. Thus,

$$Q = \dot{m}_h C_{P,h}(T_{in} - T_{out}) \tag{5}$$

The heat transfer rate is connected to the inlet and outlet temperatures and the overall heat transfer coefficient by the expression

$$Q = UA(\Delta T)_{ln} \tag{6}$$

where $(\Delta T)_{ln}$ is the log-mean temperature difference. The thermal performance of the two streams is assumed to be described by the respective heat transfer coefficients, which are related to the overall coefficient according to

$$\frac{1}{U} = \frac{1}{h_h} + \frac{\Delta x}{k_{ss}} + \frac{1}{h_c} \tag{7}$$

Term Δx is the plate sheet thickness and k_{ss} is the thermal conductivity of stainless steel.

The exchanger is first tested in single-phase operation by introducing pure water as the cold stream as well. This series of measurements is analyzed by a variant of the modified Wilson plot technique (to be described in Section 5.1) in order to extract an accurate correlation for the single-phase heat transfer coefficient of the available plate heat exchanger. Thus, a baseline for comparing the performance under two-phase flow conditions is established.

In two-phase flow operation, the heat transfer coefficient of the cold stream, h_c, is the parameter of interest and is calculated as follows: We use the measured mass flow rates and inlet/outlet temperatures to calculate the overall heat transfer coefficient, U, from Eqs. (5) and (6). Then, we apply the single-phase correlation in order to estimate the heat transfer coefficient, h_h, of the hot water stream and finally calculate h_c from Eq. (7).

A complication in data analysis under two-phase flow operation is caused by the evaporation of a small amount of the cold water during passage through the exchanger. As a result, the energy balance of the cold air/water stream cannot be calculated independently, and the heat loads reported are based only on the hot, single-phase water stream. However, given that the cold and hot stream heat loads calculated under single-phase water/water operation never deviate more than 5% from their average, we are also confident about the results under two-phase flow conditions.

The impact of evaporation on the total heat load is estimated by applying Eq. (5) separately for the air and water flow rate in the cold stream (thus ignoring the latent heat of evaporation) and comparing the result with the higher heat load calculated from the hot stream. The conclusion is that water evaporation during heating of the air/water mixture is a second-order effect, with its impact on the total heat transfer rate being far less than 10% for most of the data. Thus, an alternative method of analysis based on an enthalpy driving force (as in the Threlkeld (1970) method) was not deemed necessary.

To optimize the accuracy of the calculated heat transfer rates in view of the above limitations, we adopt the following compromise: we choose the hot water mass flow rate to be low enough to ensure a typical entrance-to-exit temperature drop of 5 °C. Simultaneously, the flow rate is kept high enough to avoid rendering its thermal resistance dominant, and thus invalidating the accuracy of h_c as calculated from Eq. (7).

4. Observations of flow regimes

Based on visual observations as recorded by the high-speed camera, a flow regime map has been compiled and is shown in Fig. 3. Four major flow regimes are identified, designated in the flow regime map as A, AB (or BA), B and C. The map is drawn in terms of superficial gas and liquid velocities, calculated according to Eqs. (1) and (2).

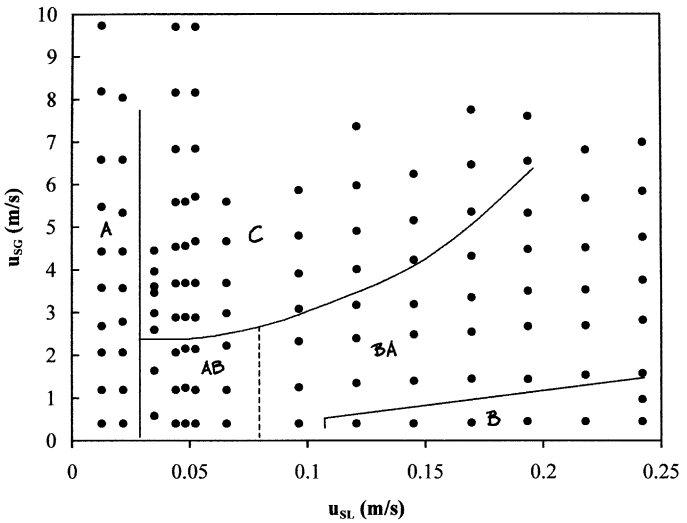

Fig. 3. The flow regime map for air/water down flow in a channel of the plate heat exchanger.

Flow regime A corresponds to liquid superficial velocity below 0.025 m/s and a wide range of gas flow rates. A typical image from regime A is shown in Fig. 4. The liquid mainly moves in the form of rivulets at the bottom of the corrugation furrows, leaving most of the channel space for a continuous gas phase. At lower gas flow rates the flow in each furrow is mainly unidirectional and the liquid is reflected at the side-walls of the channel. With increasing gas flow rate the rivulet flow is gradually observed to shift to a helical pattern, with the liquid reflecting close to the nodes where the adjacent plates are in contact. The flow then consists of a succession of jumps from a trough on one side to a trough on the other side of the channel. The liquid bridges, formed over the corrugation crests during this process, are vaguely discerned in a still picture but are more easily identified in the motion picture.

The above observations may be put into perspective with the patterns of single-phase flow, delineated by Focke and Knibbe (1986). These authors were the first to document by flow visualization the unidirectional and the helical motion inside the furrows, and found that a transition from one to the other occurs by increasing the angle of the corrugations above 72° with respect to the flow direction. Our observations, with a single corrugation angle of 60°, indicate that air/water two-phase flow tends to favor the helical motion.

At the other extreme of the flow map in Fig. 3, regime B corresponds to low superficial air velocities (generally, $u_{SG} < 1$ m/s) and to superficial water velocity above 0.1 m/s. Photos from this regime (Fig. 5) are blurry, and are in sharp contrast with Fig. 4. (A comparison of the visual appearance of flow regimes A and B is instructive for the interpretation of the rest of the data.) Fig. 5 is characterized by the absence of bright regions that would indicate a continuous gaseous phase. Thus, we conclude that the air is dispersed in the form of small bubbles inside a liquid-continuous stream that covers the entire channel space.

Keeping a constant water flow with $u_{SL} > 0.1$ m/s and increasing the airflow rate, we observe small regions occupied by gas-continuous phase to appear in a random fashion, and move downstream in the mean flow direction. An example of this pattern is shown in Fig. 6a. (Note that

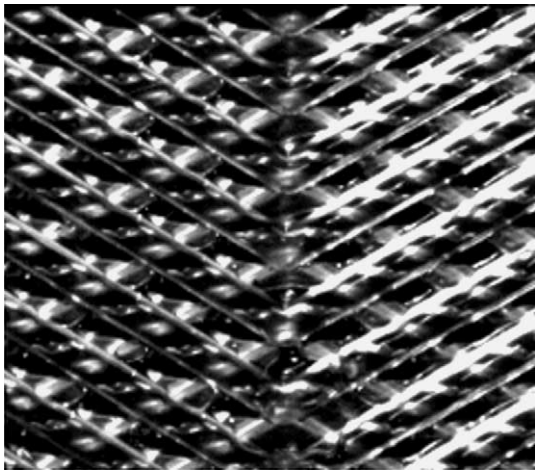

Fig. 4. Representative image of flow regime A.

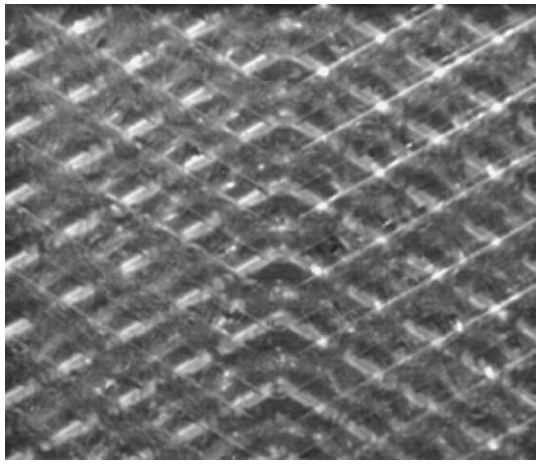

Fig. 5. Representative image of flow regime B.

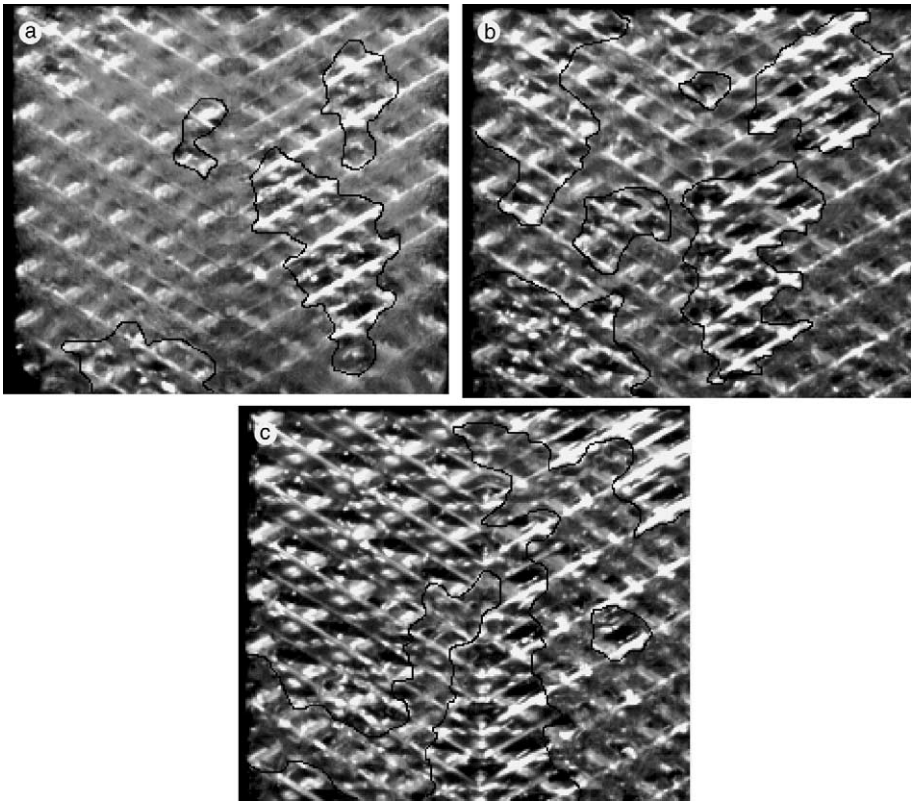

Fig. 6. (a, b) Images of flow regime BA and (c) flow regime AB (lines have been drawn artificially around the gas-continuous patches in order to facilitate the readers perception).

the lines around the gas-continuous patches are drawn artificially, in order to facilitate the readers perception of the photo.) Observation of the motion picture shows that the pattern of transport of the gas phase involves the previously described helical path with continuous changes of direction. With increasing air flow rate, the gas-continuous pockets grow in number and are distributed irregularly throughout the window of view (Fig. 6b). The motion picture reveals that the distribution is also irregular in time, with the patches segregated in low-frequency surges. The above pattern of flow is indicated in Fig. 3 as flow regime BA.

Starting again with a constant superficial air velocity below 2 m/s, and increasing the water superficial velocity above 0.025 m/s (which is the limit of flow regime A), we observe the appearance of liquid pockets within a gas-continuous phase (Fig. 6c). This regime is indicated in Fig. 3 as AB. The liquid pockets are less coherent than their gas counterparts in regime BA, and seem to occur by local flooding at neighboring nodes. As expected, the distinction between a predominantly liquid-continuous phase (BA) and a predominantly gas-continuous phase (AB) is highly subjective at the intermediate region, and the respective boundary (indicated by a dashed line in Fig. 3) is of minor importance.

Finally, at water superficial velocities above 0.025 m/s and at sufficiently high air flow rates, a slug flow regime (C) is observed. Slugs are identified by a rather sharp front, which extends over the entire width of the channel and separates a liquid continuous (B-like) region from a preceding gas continuous (A-like) region. Examples of this front are demonstrated in Fig. 7a and b (where, again, lines have been drawn to facilitate the reader's perception). The slug fronts are horizontal or slightly inclined, so as to form an approximately right angle with the direction defined by the entrance and exit ports.

At lower water flow rates, slugs extend over 1–2 corrugation wavelengths and appear as blurry ribbons (Fig. 7a). Increasing the liquid flow rate leads to an increase of the length of each slug, which is a result of the larger masses of water that need to be accommodated. However, a coherent structure is not retained over the entire length of the periodic phenomenon. Instead, the rather sharp front with a compact liquid-continuous region extends into 3–6 corrugation wavelengths, and is followed by a highly irregular region with smaller slugs and patches of the A and the B regimes. Fig. 7b and c shows respectively the front and the structure following immediately behind.

The velocity of the slugs is distinctively higher than the superficial liquid velocity, and somewhat smaller than the superficial gas velocity. For example, Fig. 7a corresponds to $u_{SL} = 0.044$ m/s, $u_{SG} = 5.6$ m/s and the average slug velocity is 2.8–3.1 m/s. Similarly, Fig. 7b comes from an experiment with $u_{SL} = 0.096$ m/s, $u_{SG} = 5.9$ m/s, and the average slug velocity is 3.8–4.1 m/s. The difference between the superficial gas velocity and the slug velocity is generally higher the lower the liquid flow rate (i.e. the shorter the slug). Thus, this difference is tentatively attributed to the aeration of the slugs, which results in air moving through the slug body in the form of bubbles (shorter slugs yield more easily to air penetration, and thus are accelerated less).

Establishment of the slug flow regime is found to be sensitive to the inlet conditions. The general influence of mixer design in the characteristics of the ensuing flow is a well-established fact in the literature and has been repeatedly demonstrated in diverse two-phase flow experiments. In the present study, the inlet consists of a horizontal pipe with i.d. = 36 mm, and we have observed that the transition between flow regimes A and C is related to the onset of slugging in the inlet port. (This is born out by visual observation of the inlet port through the transparent plexiglass

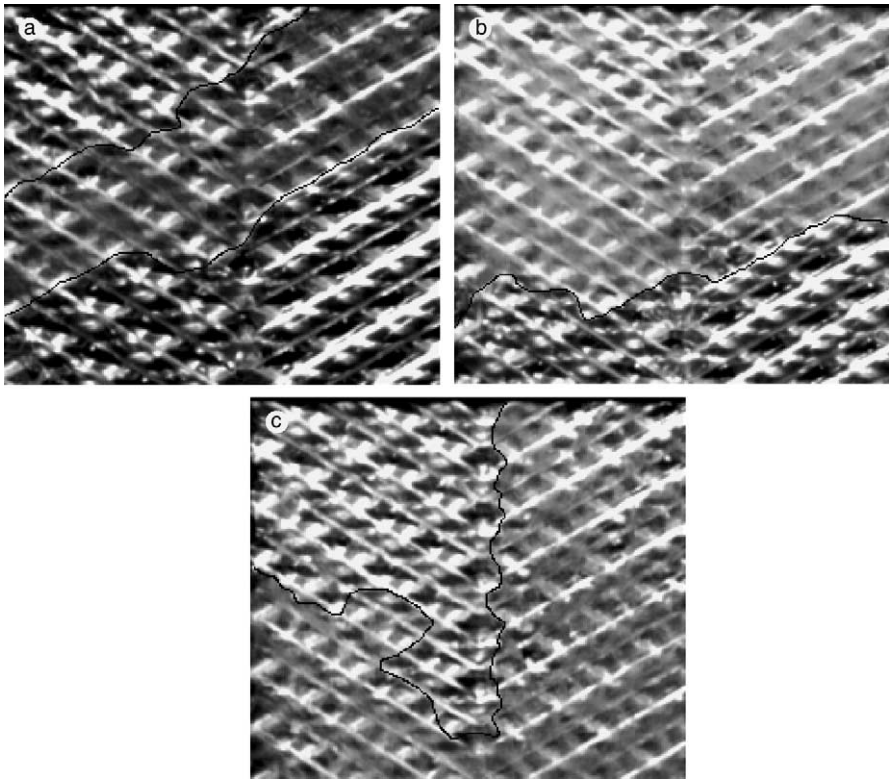

Fig. 7. (a) Images of a short slug and (b, c) a longer slug with its tail (lines have been drawn artificially at the boundary between the gas-continuous and the liquid-continuous region in order to facilitate the readers perception).

cover.) It should be noted, however, that the superficial liquid velocity inside the heat exchanger depends strongly on the number of plates used (through Eq. (1)), in contrast to the conditions at the inlet port which remain roughly the same. Thus, a systematic investigation of the role of the inlet configuration should include consideration of the effect of the number of plates used, a study not undertaken in the present work. It has also been observed that slug occurrence at the inlet port is not a sufficient condition for the occurrence of slug flow inside the plate heat exchanger. Indeed, at gas superficial velocities below 2 m/s, the liquid slug observed at the inlet pipe breaks up into liquid blobs that are not large enough to bridge the entire cross-section of the plate channel and are convected with the gas flow (regime AB).

5. Heat transfer measurements

5.1. Single-phase heat transfer

Next, we wish to derive a correlation for single-phase heat transfer, applicable to the plate heat exchanger at hand. The goal is twofold: first, we shall use this correlation under two-phase flow

operation to estimate the heat transfer coefficient of the single-phase heating stream (hot water). Second, we shall use it as a baseline for calculating the change in heat transfer accomplished by the introduction of air in the cold water stream.

In order to measure the single-phase heat transfer coefficient we use the following procedure, which may be viewed as an extension of the modified Wilson plot technique (Shah, 1985) exploiting the symmetry in the two streams in the 1-1 configuration of the plate heat exchanger: we introduce equal mass flow rates of pure water on the two sides of the exchanger. In the present, single-pass, configuration both the geometry of the passages and the flow cross-sections are identical on the two sides. Thus, the ratio of the heat transfer coefficients of the cold and the hot stream is only a function of physical properties. In particular, by positing a correlation of the form $Nu = aRe^{b}Pr^{1/3}$ and by neglecting variations in water density and specific heat, we obtain

$$\frac{h_c}{h_h} = \left(\frac{k_c}{k_h}\right)^{2/3}\left(\frac{\mu_h}{\mu_c}\right)^{b-1/3} = \alpha \tag{8}$$

where physical properties are evaluated at the arithmetic average of the entrance and exit temperatures of each stream.

Substituting Eq. (8) in Eq. (7), we obtain

$$h_h = \frac{1 + 1/\alpha}{1/U - \Delta x/k_{ss}} \tag{9}$$

We use Eq. (9) to arrive at a best-fit prediction of b by a trial-and-error procedure. First, we make the rough assumption that $\alpha \approx 1$, calculate h_h from (9) and choose two values of b , in order to fit the low and high-Re data respectively as function of the Reynolds number. Using the first estimates of b, we update the value of α from (8) and repeat the calculation. One or two iterations are sufficient for convergence.

The correlations obtained by the above procedure are

$$Nu = 0.000672Re^{1.6}Pr^{0.33} \quad \text{for } Re < 650 \tag{10a}$$

$$Nu = 0.51Re^{0.58}Pr^{0.33} \quad \text{for } Re > 650 \tag{10b}$$

and are shown, together with the measurements in Fig. 8. Maximum spread of the data is ±6%, in agreement with expectations based on an uncertainty analysis. According to the above data fit, the lower limit of fully developed turbulent flow is estimated as $Re \approx 650$.

The exponent of the Reynolds number in (10b) agrees with the correlation proposed for turbulent flow through a plate heat exchanger by Chisholm and Wanniarachchi (1991). However, the low-Re data deviate remarkably from the classical Leveque correlation for circular conduits ($Nu \sim Re^{1/3}$), which has also been proposed (Bond, 1981) as suitable for plate heat exchangers. Though the 1.6 exponent of the laminar correlation is unexpected, the scatter in the data is very small and their reproducibility has been repeatedly confirmed.

The multipliers in (10a) and (10b) are known (Shah and Wanniarachchi, 1991) to depend on the corrugation geometry and—for developing, laminar flow—also on the length of the plate. Since we are presently testing only one type of plate, no further investigation of these dependencies is attempted.

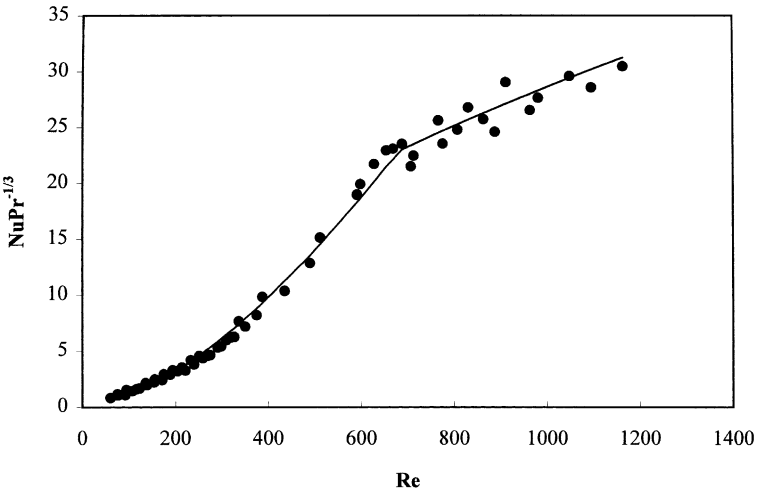

Fig. 8. The data (···) and the correlation (—) for single-phase heat transfer in the P-01 plate heat exchanger.

5.2. Two-phase heat transfer

Next, we wish to consider the dependence of the heat transfer coefficient of the air–water stream on the flow rates of the two phases, using as baseline the single-phase operation with water only. Our goal at the present stage is mainly exploratory: we want to identify the respective trends and to question their possible relation to the prevailing flow regime. Measurements of the two-phase heat transfer coefficient are shown in Fig. 9. The ordinate is the superficial cold water velocity, u_{SL},

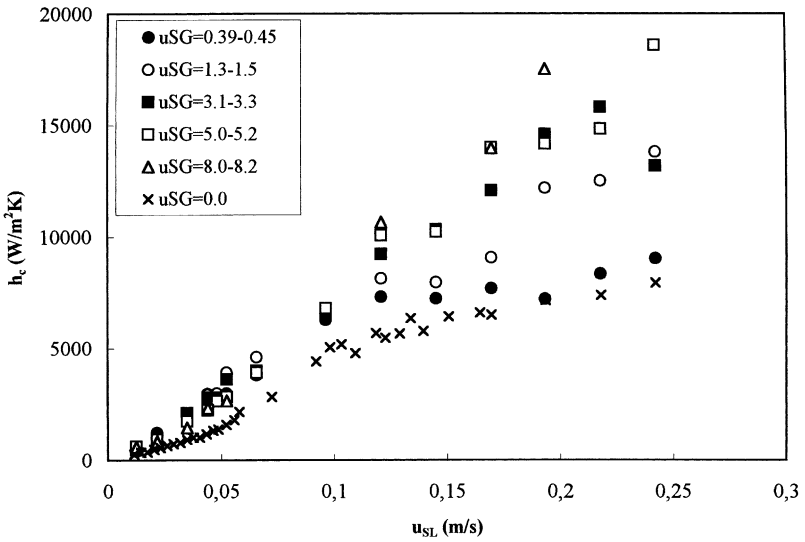

Fig. 9. Measured air–water heat transfer coefficient as a function of superficial water velocity, for different superficial air velocities.

and each series of data refers to a narrow range of superficial air velocities, u_{SG} (because of the dependence of the air pressure on flow rate, it is not easy to perform different experiments at precisely the same superficial air velocity). Using the above parameters, heat transfer data may be set in perspective with the flow regime map of Fig. 3.

According to Fig. 9, the two-phase heat transfer coefficient is an increasing function of water flow rate. However, the impact of the co-current airflow is non-trivial and proves to be interesting. A first observation is that, in the range of superficial air velocities examined, air always has a positive effect on the heat transfer coefficient, i.e. measured values are higher than those corresponding to the same water flow rate but without air (Data for single-phase operation are included in Fig. 9 for comparison. They are similar in shape to Fig. 8 and, in particular, exhibit a laminar-turbulent transition around a superficial liquid velocity $u_{SL} = 0.1$ m/s). This effect of co-current airflow should be contrasted with common operation practice, where small amounts of non-condensable gases affect adversely the operation of heat exchangers by reducing the area available for heat transfer. The present data indicate that a minimum superficial air velocity $u_{SG} = 0.4$ m/s is sufficient to overcome the aforementioned gas-blanketing effect and actually to enhance heat transfer. A candidate mechanism for this enhancement will be suggested later.

The behavior at low and at high superficial water velocities merits separate consideration. Fig. 9 indicates that, for u_{SL} in the range 0.01–0.1 m/s, measured values of the heat transfer coefficient are relatively insensitive to the air superficial velocity. On the contrary, for u_{SL} in the range 0.1–0.25 m/s, there is observed a direct effect of the superficial air velocity. An alternative way of viewing these data is by plotting the enhancement in the heat transfer coefficient, i.e. the ratio of the values measured, for the same water flow rate, under two-phase and single-phase operation. The data in this form are shown in Fig. 10.

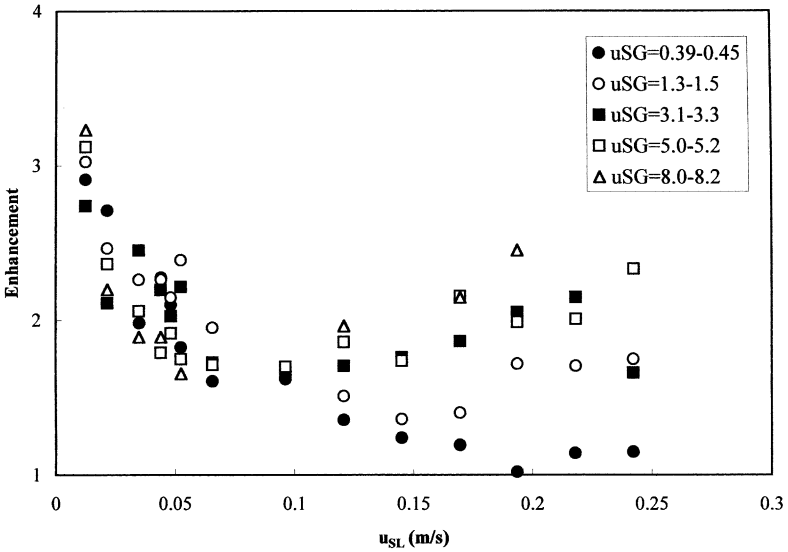

Fig. 10. Enhancement of the heat transfer coefficient (over the value measured with water only) as function of the superficial air and water velocities.

The above information can be related to the observed flow regimes (Fig. 3) as follows: Fig. 10 shows that the highest enhancement occurs at superficial water velocities below $u_{SL} = 0.025$ m/s and for the entire range of superficial air velocities considered. These conditions correspond to flow regime A, which involves a continuous gaseous phase covering the core of the channel and a liquid phase moving in the form of rivulets inside the corrugation furrows. The observed enhancement of heat transfer by the air flow may be attributed to the shear exercised by the air on the water film. In particular, Focke et al. (1985) and Focke and Knibbe (1986) have shown that the criss-crossing paths of the furrows of adjacent plates inside the same channel result in the development of secondary swirling motions which enhance heat transfer under single-phase operation. Similarly, the flow of air through the channel must necessarily follow one of the two possible routes (i.e. unidirectional with reflections on the walls or helical with reflections at the nodes). In either case, it exerts a co-current shear on the liquid inside one furrow and a swirling shear on the liquid in the opposite furrow. As the enhancement observed for $u_{SL} < 0.1$ m/s is roughly independent of air superficial velocity, we may conclude that there is a plateau behavior with the minimum superficial air velocity presently tested ($u_{SG} = 0.4$ m/s) being sufficient to trigger the full effect.

For the data with $u_{SL} > 0.1$ m/s, both Figs. 9 and 10 indicate that the lowest superficial air velocity, $u_{SG} = 0.4$ m/s, results in marginal improvement over single-phase operation. Note that these conditions correspond to flow regime B, which thus appears as not particularly favorable for heat transfer. Increasing the superficial air velocity, so as to enter the BA flow regime, leads to a gradual improvement in heat transfer efficiency. Finally, there is no evident distinct effect associated with the transition to slug flow. At any rate, the enhancement observed in flow regime A is only approached by a combination of the highest superficial velocities of both phases. Operation under the latter conditions is expected to result in a severe pressure drop penalty compared to operation in flow regime A.

6. Concluding remarks

A plate heat exchanger is tested under two-phase flow conditions by using an air/water mixture as the cold stream. Visual observations lead to the identification of different flow regimes: at water superficial velocities below 0.025 m/s the liquid resides inside the bottom of the furrows and is sheared by a continuous gas phase (regime A). At superficial water velocity above 0.1 m/s and low air velocities, a liquid-continuous phase covers the entire channel area (regime B). At intermediate-to-high superficial velocities of both phases the flow regime is either a combination of the above (regimes AB and BA), or genuine slug flow. Establishment of the latter seems to be affected by the arrival of slugs at the entrance pipe.

For all superficial air velocities tested, the heat transfer coefficient of the air/water stream is always higher than the coefficient corresponding to the same water flow but with no air. The observed enhancement is more significant at low superficial water velocities and supports the argument that flow regime A is the most efficient for heat transfer.

The detailed characteristics of the gas-sheared rivulet flow occurring in regime A are to a large extent unknown. An interesting question, which we are not presently able to answer, is whether

the exchanger plates are only partially wetted in this regime or whether a thin liquid layer is actually sustained everywhere (possibly supported by droplet deposition from the gas stream). It is reasonable to expect that the answer to this question will also depend on the wetting characteristics of the plate material. Local film thickness measurements by a conductivity probe would provide valuable information in this direction.

Acknowledgements

The authors are indebted to α-Laval for donating the heat exchanger used in this study.

References

Bansal, B., Müller-Steinhagen, H., 1993. Crystallization fouling in plate heat exchangers. ASME J. Heat Transfer 115, 584–591.

Bond, M.P., 1981. Plate heat exchangers for effective heat transfer. Chem. Engng. 9, 162–166.

Bontozoglou, V., Papapolymerou, G., 1997. Laminar film flow down a wavy incline. Int. J. Multiphase Flow 23, 67–79.

Bontozoglou, V., Papapolymerou, G., 1998. Wall-triggered interfacial resonance in laminar gas–liquid flow. Int. J. Multiphase Flow 24, 131–143.

Buonopane, R.A., Troupe, R.A., Morgan, X.X., 1963. Heat transfer design method for plate heat exchangers. Chem. Engng. Progr. 59, 57–61.

Carlson, J.A., 1992. Understanding the capabilities of plate-and-frame heat exchangers. Chem. Engng. Progr. 59, 26–31.

Chisholm, D., Wanniarachchi, A.S., 1991. Layout of plate heat exchangers. In: ASME/JSME Thermal Engineering Proceedings, vol. 4. ASME, New York, pp. 433–438.

Cooper, A., Usher, J.D., 1983. Plate heat exchangers. In: Schlunder, E.U. (Ed.), Heat Exchanger Design Handbook, vol. 3. Hemisphere, Washington.

Focke, W.W., Knibbe, P.G., 1986. Flow visualization in parallel-plate ducts with corrugated walls. J. Fluid Mech. 165, 73–77.

Focke, W.W., Zachariades, J., Olivier, I., 1985. The effect of the corrugation inclination angle on the thermohydraulic performance of plate heat exchangers. Int. J. Heat Mass Transf. 28, 1469–1497.

Gradeck, M., Lebouché, M., 2000. Two-phase gas–liquid flow in horizontal corrugated channels. Int. J. Multiphase Flow 26, 435–443.

Malamataris, N., Bontozoglou, V., 1999. Computer aided analysis of viscous film flow along an inclined wavy wall. J. Comptat. Phys. 154, 372–392.

Marriott, J., 1971. Where and how to use plate heat exchangers. Chem. Engng. 78, 127–133.

Patel, N., Thompson, P., 1991. Plate heat exchangers for process evaporation and condensation. In: Sharp, D. (Ed.), Heat Exchange Engineering, vol. 2. Ellis Horwood, New York, pp. 385–397.

Raju, K.S.N., Bansal, J.C., 1983. Design of plate heat exchangers. In: Kakac, S., et al. (Eds.), Low Reynolds Number Flow Heat Exchangers. Hemisphere, Washington, pp. 913–932.

Shah, R.K., 1985. Compact heat exchangers. In: Rohsenow, W.M., Partnett, J.P., Ganic, E.N. (Eds.), Handbook of Heat Transfer Applications. McGraw-Hill, New York, pp. 209–212.

Shah, R.K., Focke, W.W., 1988. Plate heat exchangers and their design theory. In: Shah, R.K., et al. (Eds.), Heat Transfer Equipment Design. Hemisphere, Washington, pp. 227–254.

Shah, R.K., Wanniarachchi, A.S., 1991. Plate heat exchanger design theory. In: Buchlin, J.-M. (Ed.), Industrial Heat Exchangers, vonKarman Institute Lecture Series 1991-04.

Shetty, S., Cerro, R.L., 1993. Flow of a thin film over a periodic surface. Int. J. Multiphase Flow 19, 1013–1027.

Threlkeld, J.L., 1970. Thermal Environmental Engineering. Prentice-Hall, New York.
Trifonov, Yu.Ya., 1998. Viscous liquid film flow over a periodic surface. Int. J. Multiphase Flow 24, 1139–1161.
Usher, J.D., 1970. Evaluation of plate heat exchangers. Chem. Engng. 62, 90–94.
Walker, G., 1982. Plate heat exchangers. In: Industrial Heat Exchangers. Hemisphere, Washington, pp. 87–113.